Responses to reviewers for "Tropical Continental Downdraft Characteristics: Mesoscale Systems versus Unorganized Convection" by K. A. Schiro and J. D. Neelin

Reviewer #1

1. It's worth mentioning that the analysis was focused on the more extreme convection, consisting of 11 isolated cells and 17 MCSs. A sentence discussing the differences between the isolated and organized convection cases would also be useful.

Thanks, in the abstract line 11 we added the word "strong" to clarify. Additionally, lines 14-17 were modified to elaborate on similarities and differences between MCSs and isolated cells.

2. line 88: 30-minutes strikes me as a long time-span over which to average cold pool changes, which those changes easily happening over shorter time spans. Why did the authors choose this time scale? can they say something here about the ability to resolve temporal evolution? on line 137 you mention averaging over 1 hour, even longer.

We originally chose 30 minutes for these types of composites because otherwise it is difficult to condition on a distinct decrease in θ_e. If conditioning on, say, 5 min average decreases in θ_e, the decrease in θ_e observed over that period of time may not be unlike usual fluctuations in θ_e throughout the diurnal cycle. On the other hand, large decrease in θ_e over a 15 or 30 minute timeframe are frequently attributable to the passage of a cold pool. We have modified Fig. 2 to include composites of 5 min average quantities, yet we still condition on the decreases in θ_e of >=5K and precipitation rates >= 10 mm/hr over a 30 minute time period, as was originally the case for the aforementioned reason.

3. were all of the cold pools preceded by unmodified conditions? cold pools tend to cluster.

It is difficult to say with certainty whether the cold pools were preceded by unmodified conditions; the composites do not show any significant precipitation occurring beforehand, however, and thus we do not suspect that the surface thermodynamics had been appreciably modified by precipitation or cold pools.

4. discussion of Figs 2 and 3: do the individual examples all follow the same evolution as is shown for the mean composite?

The evolution can vary to some degree. We try to illustrate this evolution with shading (+/- 1 std. dev.), which are calculated with respect to the value of minimum θ_e within a cold pool (discussed in lines 131-133). Additionally, for visual clarity, we shifted the minimum θ_e to time 0 in Fig. 2.

5. lines 199-200, fig. 3: it is difficult to discern a difference of 700m between 2 separate plots extending up to 17km. I would encourage the authors to try out different plotting formats, perhaps one plot showing both of the mean profiles together up to 17km, and another one zoomed in to the 0-4km range would work, showing all 6 mixing lines. This would help with interpretation of the mixing rates and their differences for the two forms of convection, as discussed in lines 215-225, as well.

Thanks for this suggestion. We restricted the height to 7 km to zoom in on the features in the lowest levels more closely.

6. line 242-243: it is difficult to see the downdraft this sentence is referring to in Fig. 5. perhaps an arrow, or a color scheme emphasizing the stronger downdrafts, would help. the latter might be my suggestion, to use e.g. red for downdrafts less than -1 m/s and yellow for updrafts > 1 m/s. or vice versa, in which case you might have something that relates well to the probability of downdrafts figure in the bottom panel.

I also wonder if it would be useful to blow up the 0-4km altitude range in Figs 5 and 6. The manuscript makes the argument that downdrafts originate from the lower free troposphere, but these figures focus the eye on the upper troposphere. I have trouble distinguishing features mentioned in the text (e.g., lines 260-261) in the figures. One idea might be to make this 6-paneled figures with 3 additional panels added per figure that focus on the 0-5km range.

We added two additional panels in Figs. 4-5 (old Figs. 5-6) to zoom in on the 0-4 km region to emphasize the downdrafts being discussed in the text.

7. p. 9: I see no discussion of wind shear here. What role if any does the (horizontal) wind profile play in this? line 260-261 would suggest none, is this consistent with conceptual views of MCS organization?

We did not evaluate the effects of wind shear on MCS organization and downdrafts, although it is known to play an important role. Our goal here was to estimate downdraft origin height for the downdrafts associated with the initial sharp drop in θ_e at the surface. We would expect that wind shear is important to these MCSs and their downdrafts, as moderate shear is known to be favorable for the development of MCSs (e.g. Wesiman and Klemp 1982; Rotunno et al. 1988), but we cannot comment on the effects of wind shear on updraft or downdraft properties from the analysis presented.

8. line 256: how can downdraft air be positively buoyant? does it overshoot its level of neutral buoyancy?

This discussion is referring to the results in Sun et al. (1993). Because they are a dynamical response to the updraft, they are dynamically pushed downwards, but would otherwise be thermodynamically unstable (i.e., positively buoyant). See Sun et al. (1993) for a comprehensive discussion.

9. line 263: I have trouble distinguishing this feature. is this occurring between 1-2 hours near the surface?

We have modified this sentence accordingly in lines 276-279, as it is a bit difficult to see from the composites (although they more than likely exist).

10. lines 283-296: see also de Szoeke et al 2017 JAS for further corroborating observations from DYNAMO.

Thank you. We added this reference to support the discussion in line 309.

11. lines 359-361: I wonder if sampling can explain why you might find a strong precipitation event without a decrease in surface θ_e, as it doesn't quite make sense to me that this would be the case, unless the decrease in surface θ_e is simply displaced.

Displacement is possible, but the results presented suggest that it does not greatly affect the results. For instance, we tested to see whether θ_e is displaced from precipitation (e.g. large decreases in θ_e without appreciable precipitation) using radar data in Fig. 7. This does not modify the distribution of precipitating points as a function of $\Delta\theta_e$ or the probability curve very much, suggesting that the in situ $\Delta\theta_e$ and precipitation correspond well to one another (we commented on this in lines 364-366). So it is likely, as shown in the distribution of precipitating points and other evidence from Figs. 3-6 that downdrafts commonly originate at low enough levels where the decrease in θ_e is small (or they mix considerably enough to make the decrease negligible).

Another thing to consider is displacement in time. In Figs. 7 and 8, the statistics are compiled based on 1-h average values of $\Delta\theta_e$ and precipitation. When we bin and conditionally average the precipitation by $\Delta\theta_e$ we only condition based on events occurring within that hour. The 1-h interval was chosen to hopefully be a coarse enough resolution to capture the $\Delta\theta_e$ from a cold pool in one time step, yet a high enough resolution to retain the signal despite averaging. We suspected, however, that this interval might not be wide enough to capture all precipitation that falls with each system in any given hour. So in Fig. 9, we try to avoid this as best as possible by instead conditioning on the maximum precipitation rates and minimum $\Delta\theta_e$ (1-hr average values) within a given 3 hour interval. Nevertheless, from what we can tell, the results do not appear very sensitive to displacements in space or time, thus confirming that there are modest $\Delta\theta_e$ decreases that occur without coincident precipitation (and vice versa) and that displacement is not playing a major role.

There is also some dependence on the threshold θ_e decrease chosen to define cold pools (e.g. in Fig. 9 and in the stats presented in lines 409-414), though we feel that -2 K is appropriate. The variance of $\Delta\theta_e$ is 3.12 (mean is ~0) and the standard deviation is 1.76, so we chose -2 to be below 1 σ.

12. line 45: Zuidema et al 2011 should be Zuidema et al 2012

Thanks. This has been corrected.

13. line 71: provides should be provide

Corrected. Please see tracked changes.

14. line 140-141: the language here is slightly unclear ("drops of -5C or less"). would suggest referencing to an absolute value.

Corrected. Please see tracked changes.

15. line 167: typo at end

Corrected. Please see tracked changes.

16. line 257: mention the gravity waves are in the stratosphere

Corrected. Please see tracked changes.

1. (Abstract) line 18 : change 'have a probability' to 'have a probability of occurrence' -The abstract is too long. Please reduce it. I propose to suppress the sentence from l 20 to l 23. -You should also reformulate the end of the abstract after l28 which is unclear.

We have reduced the abstract and clarified as needed, per this suggestion. Please see tracked changes for specifics.

2. (Introduction) This section could refer more to previous studies that use observations to document cold pools. Here are a few examples of reference missing: Charba, 1974; Engerer et al, 2008; Feng et al 2015; Redl et al 2015. Some are quoted in the rest of the text but this section should provide an overview of what we know about downdrafts from observations.

We have added some additional references to this section, as suggested.

3. (Data & Methods) Line 115: 'that create a subsequent drop in θ_e at the surface of less than -5 C': (also line 140 and line 167) How is the drop quantified? Over which time interval? Please be more specific.

Thanks for pointing this out. The drops are quantified within a 30-min interval. The θ_e from the previous interval is subtracted from the following interval, which defines the $\Delta\theta_e$. If that $\Delta\theta_e$ is less than –5 K (and precipitation is greater than 10 mm hr^{-1}) we include the convective event in our composite. We clarified this in lines 103-105.

4. From Fig 2, it seems that the drop is more than -5°C. And This is also indicated in l148 to 150: 'Values of θ_e are 353.6K on average before passage of the cell. An hour after the passage, the θ_e value drops by an average of 8.9° to an average value of 344.7K'

Yes, we condition on events with depressions greater than 5 K, which is why the composites show values greater than 5 K.

5. Also please mention here than no latent heat flux measurements are available at the passage of the convective systems and the following hour.
6. The surface flux panels are not commented in the text so either removed them from Fig 2 and 3 or comment them.

We have removed the surface flux panels in the main text, with brief discussion about this issue, and have moved them to the SI (Figs. S1 and S2).

7. Please indicate how the recovery time is computed.

Yes, thanks. Please see tracked changes (lines 135-138).

8. (Surface thermodynamics) lines 174-175: please indicate also the average value of CWV for the isolated cells. For the MCS, please compare the figure showing the evolution of the CWV with Figure 3 of Taylor et al (2017).

We added the values for more quantitative comparison, as suggested, and have compared to Taylor et al. (2017).

9. (Downdraft origin and the effects of mixing) The 1.3km and 2km for the origin of the downdraft with the assumption of no-mixing is only derived for one given case? Or is obtained from the composite of all the radiosondes for a given category? Could you please comment on the range of values obtained for all the cases and change Figure 4 by one figure showing the mean profile +/- the standard deviation.

This is the mean of all profiles in a given category, and we compute the mixing from the mean profile. We added to the text in lines 202-206 for clarification. We also modified the figure to add error bars (+/- 1 standard error).

10. (Vertical velocity and downdraft probability) This section is a bit short on conclusion ('These results suggest that in most downdrafts, a substantial fraction of the air reaching the surface originates in the lowest 3km'). According to Figure 7, above 3km there is still a probability of ~0.4 to get a downdraft.

We have modified this wording in lines 305-307 as follows: "These results, and those presented in the previous section, suggest a range of downdraft origin levels throughout the lowest few kilometers within both organized and unorganized convective systems."

11. Also, Fig 5, 6 and 7 do not show much details in the lower levels you may want to zoom this figure in the lower 7 or 10 km.

We have zoomed Figs. 3-5 per this suggestion.

12. please comment on the dispersion on reflectivity and vertical velocity obtained for the different individual cases.

We rearranged and added to the discussion surrounding Fig. 6 to help clarify the methods, and added a discussion in lines 300-304 to place bounds on the variability observed.

13. line 328 change 'in Fig 5' to 'in Fig 4' –

Thanks; this has been corrected.

14. How do you interpret the fact that you have some points with very large negative anomaly (<15°) in equivalent potential temperature and no precipitation?

We have since eliminated these points from the figures since we tightened the constraints on the counts required to produce a robust signal (minimum counts: 5).

15. Please indicate that the $\Delta\theta_e$ is always the same one, i.e. determined from in-situ observations.

A sentence was added (line 352-353) to clarify this.

16. l357-359: minimum or maximum of $\Delta\theta_e$: please make it clearer. :'The MAXIMUM of Dtheta_e within a 3-h window of a given precipitation rate is averaged to minimize the effects of local precipitation maxima occurring slightly before or after the MINIMUM in $\Delta\theta_e$'.

Thanks for pointing this out. We have revised this wording. Please see tracked changes.

17. Please detail more how those diagnostics could be used as a constraint for parameterization.

Thanks for the suggestion. We elaborated on this in lines 405-414.

18. (Conclusions) Temperature drop of 3.9°C or 4.4° and Equivalent potential temperature from of 8° or 8.9° (line 154 or line 381) for isolated cells: please be consistent. Also check the values for the MCS cases: they are in consistent in the text and the conclusion –

We have checked this for consistency and reported the correct values in both places. Thanks for pointing this out.

19. 'with the moisture recovering faster than temperature': do you have an assumption to explain such feature.

We suspect that after the storm passes, the persistence of clouds hinders an immediate increase of heating, yet increased evaporation from the wet surface can increase the moisture content. We added a brief discussion to lines 157-161 to address this.

20. L 411: 'For area-averaged precipitation on scales typical of GCM grids, precipitation magnitude is lower for strong, negative $\Delta\theta_e$, consistent with the points with large $\Delta\theta_e$ occurring at localized downdraft loca- tions within a larger system with smaller area-average precipitation': I don't get the argument: why the $\Delta\theta_e$ will not also be smaller in this case?

The $\Delta\theta_e$ we use is in situ; we do not have any spatial information. The area-averaged precipitation decreases with increasing area, but we don't have the ability to scale up the $\Delta\theta_e$.

21. (Figure 1) Please provide in the caption the name of the field that is drawn and its unity

Corrected. The field is reflectivity (dBZ).

22. (Figure 2) It will help the lecture of this graph if there were some horizontal lines for the values as shown in the upper panel of Figure 5. Otherwise, it is very difficult to get a quantitative information from these subplots. In the caption, you mention overbars, in fact there are only drawn for the precipitation; for the other parameters, a shading is indicated around the mean: please modify accordingly the caption.

We have modified the figure according to your suggestion.

23. (Figure 3) to help in the comparison please add the mean values of Figure 2 on Figure 3 with a dashed line.

Thanks for this suggestion. We combined Figs. 2 and 3 based on this recommendation.

24. (Figure 4) I guess those profiles are from one radiosonde profile only and a given case for each case (otherwise I do not expect such small scale vertical variations of the equivalent potential temperature for an average over more than 10 radiosonde profiles). Please replace by a figure showing the mean and +/- the standard deviation shown by a shading.

These are means of the MCSs and isolated events. We have added error bars (+/- 1 standard error).

25. (Figures 5 and 6) I am impressed by the relatively un-smooth aspect of those figures for an average over 11 and 17 cases respectively. For the vertical velocity please use a red-blue colour bar in order for the reader to more rapidly identify the ascending versus descending areas.

The plots do not appear smooth because we are showing composites of high-frequency radar wind profiler data, which can be somewhat noisy. The figure has been modified to help with this. After trying multiple color bars, it seemed clearest to keep the same color bar as before, but to add panels zoomed in on the lowest 4 km for visual clarity.

26. (Figure 8) What is the unit of the right panel? Please keep the same colour legend for all subplots. –

It is a frequency of the counts of $\Delta\theta_e$, and all colors should now be consistent (now Fig. 7).

27. (Figures 9 & 10) Please add both sites on the same sub-plots and reduce the number of subplots from 3 to 6.

Thanks for the suggestion. We have modified accordingly in Fig. 8 (old Fig. 9), which is very helpful. We also tried this for Fig. 9 (old Fig. 10), but the figure became too busy.

Reviewer #3

1. Line 40: I believe the surname is actually Böing.

Yes, thank you, we have modified this.

2. Line 41-42: The boundary between the cold pool and the environment is not, strictly speaking, a mechanism. Please rephrase this.

Thanks for pointing this out. Please see tracked changes.

3. Line 149 and following: I find the use of Celsius and Kelvin at the same time confusing. Please use Kelvin throughout the manuscript.

We modified all units to be Kelvin, as suggested, and have modified the figures and text accordingly.

4. Line 149: Please specify units of measurements for 8.9.

Corrected.

5. Line 164: Could the greater recovery of the temperature be simply due to the diurnal cycle (i.e., the fact that some of the systems you are observing are in the late part of the day)?

We think it is moreso the modification to the incoming solar insolation with cloud cover and added downdrafts from the stratiform region of MCSs that sets apart the recovery times for thermodynamic variables between the MCS and isolated cases. We believe this is the case because many of the MCSs are observed in the afternoon also, and inspection of the individual events does not lead us to believe it is an artifact of the diurnal cycle. We added a short discussion of this in lines 254-258.

6. Line 187: I think "corresponding" would be a better term here.

Thank you; we agree and modified the text accordingly.

7. Line 219-220: Judging from Figure 4, the minimum of θ_e for the isolated case seems much higher than what you indicated, more like 5 km.

We are careful not to claim where the exact level of the minimum in θ_e is, as it is a little difficult to tell in this composite and can range anywhere from ~3-7 km in height. We just simply choose a point at the same height as the MCS case at the lower end of this range (3.2 km). Additionally, since the values between 3-7 km (the mean values) are relatively similar, the mixing rate will not be sensitive to the exact level of origin.

8. Line 224-229: Could you speculate whether a higher mixing rate for isolated convection would actually make sense?

This is a very good question – one that also requires thought about the actual mixing paradigm. It depends on many factors, many of which are beyond the scope of this study. It is plausible that the environment mixes differently with the surrounding environment in isolated vs. MCS events, given differences in the dynamics between storm types. It is also possible that we are not optimally characterizing the vertical profile of the thermodynamic environment, since we are compositing radiosonde measurements within hours of the observed convective event, in addition to other associated errors (e.g., sample size). The main

idea behind the analysis in Fig. 4 was to provide loose guidance for what seemed to be an appropriate degree of mixing given the current mixing paradigms employed operationally in GCMs. In response, we added to the discussion in lines 237-243 to help clarify our intention.

9. Line 248-250: You say that retrieval near freezing level has large errors, so how confident are you about the high probability you mention?

From a data quality perspective, we have greater confidence in convective regions than stratiform regions due to complex assumptions about microphysics and weaker air motions in stratiform regions. We thus restrict our main discussion and analysis to the convective regions. We have no reason to believe that we should not be confident in the quality of the retrievals in convective regions (S. Giangrande, personal communication).

10. Line 286: Betts 1976 should have parentheses?

Corrected.

11. Line 292: The altitude of 1.5 km is cited only as a reference point. The mode of the distribution seems to actually be at 1km.

Thanks. We've added "with the mode of the distribution nearer to 1 km" to line 332.

12. Line 318: The relationship in Figure 8 seems non-linear with a plateau/decrease towards lower $\Delta\theta_e$. Why is that?

This is a good question. It seems as though the higher rain rates do not necessarily correspond to colder cold pools. We are careful not to discuss this at length, as these data out to high θ_e are rare. We have since removed some of these data from the plots in Figs. 7-8, as they did not meet reasonable minimum count requirements.

13. Line 356: "The maximum $\Delta\theta_e$ [. . .]". Do you mean the minimum?

Yes, thanks. This has been corrected.

14. Line 379: Please check the number you are providing here as they don't seem in agreement with what you reported earlier on.

Thanks. We have confirmed/modified the values reported.

15. Line 381-383: Why is moisture recovering faster?
16. Line 395-396: Again, it would be very nice if you could suggest reasons why this could happen.

We suspect that after the storm passes, the persistence of clouds hinders an immediate increase of heating, yet increased evaporation from the wet surface can increase the moisture content. We added a brief discussion to lines 254-258 to address this.

17. Line 419: Do you mean "composing"?

It was supposed to be "compositing." Thanks for pointing this out; it has been corrected.

1   Tropical Continental Downdraft Characteristics: Mesoscale Systems versus Unorganized

2   Convection

3   Kathleen A. Schiro[1] and J. David Neelin[1]

4   [1]*Department of Atmospheric and Oceanic Sciences, University of California Los Angeles, Los*

5   *Angeles, CA, USA*

6   Corresponding Author: Kathleen A. Schiro, Department of Atmospheric and Oceanic Sciences,

7   University of California, Los Angeles, Box 951565, Los Angeles, CA 90095. E-mail:

8   kschiro@atmos.ucla.edu

9

10   **Abstract**

11   Downdrafts and cold pool characteristics for strong mesoscale convective systems

12   (MCSs) and isolated, unorganized deep precipitating convection are analyzed using multi-

13   instrument data from the DOE Atmospheric Radiation Measurement (ARM) GoAmazon2014/5

14   campaign. Increases in column water vapor (CWV) are observed leading convection, with higher

15   CWV preceding MCSs than for isolated cells. For both MCSs and isolated cells, increases in

16   wind speed, decreases in surface moisture and temperature, and increases in relative humidity

17   occur coincidentally with system passages. Composites of vertical velocity data and radar

18   reflectivity from a radar wind profiler show that the downdrafts associated with the sharpest

19   decreases in surface equivalent potential temperature (θ_e) have a probability of occurrence that

20   increases with decreasing height below the freezing level. Both MCSs and unorganized

21   convection show similar mean downdraft magnitudes and probabilities with height. Mixing

22   computations suggest that, on average, air originating at heights greater than 3 km must undergo

23   substantial mixing, particularly in the case of isolated cells, to match the observed cold pool θ_e,

24   implying a low typical origin level. Precipitation conditionally averaged on decreases in surface

25   equivalent potential temperature ($\Delta\theta_e$) exhibits a strong relationship because the most negative

26    $\Delta\theta_e$ values are associated with a high probability of precipitation. The more physically motivated

27   conditional average of $\Delta\theta_e$ on precipitation shows that decreases in θ_e level off with increasing

28   precipitation rate, bounded by the maximum difference between surface θ_e and its minimum in

Deleted: For both MCSs and isolated cells, there are

Deleted: the convection

Deleted: and i

Deleted: coincident

Deleted: This is consistent with thermodynamic arguments: if θ_e were approximately conserved following descent, it would imply that a large fraction of the air reaching the surface originates at altitudes in the lowest 2 km, with the probability of lower θ_e dropping exponentially.

38 the profile aloft. Robustness of these statistics observed across scales and regions suggests their

39 potential use as model diagnostic tools for the improvement of downdraft parameterizations in

40 climate models.

41 1 Introduction

42   Convective   downdrafts   involve   complex   interactions   between   dynamics,

43 thermodynamics, and microphysics across scales. They form cold pools, which are evaporatively

44 cooled areas of downdraft air that spread horizontally and can initiate convection at their leading

45 edge (Byers and Braham 1949; Purdom 1976; Wilson and Schreiber 1986; Rotunno et al. 1988;

46 Fovell and Tan 1998; Tompkins 2001; Khairoutdinov and Randall 2006; Lima and Wilson 2008;

47 Khairoutdinov et al. 2009; Böing et al. 2012; Rowe and Houze 2015). The boundary between the

48 cold pool and the surrounding environmental air, known as the outflow boundary or gust front, is

49 key to sustaining multi-cellular deep convection (e.g. Weisman and Klemp 1986). It has also

50 been shown to trigger new convective cells in marine stratocumulus clouds (Wang and Feingold

51 2009; Terai and Wood 2013) and in trade-wind cumulus (Zuidema et al. 2012; Li et al. 2014).

52 Downdrafts also have implications for new particle formation in the outflow regions, which

53 contribute to maintaining boundary layer CCN concentrations in unpolluted environments (Wang

54 et al. 2016).

55   Precipitation-driven downdrafts are primarily a result of condensate loading and the

56 evaporation of hydrometeors in unsaturated air below cloud base (e.g. Houze 1993), with

57 evaporation thought to be the main driver (Knupp and Cotton 1985; Srivastava 1987). It was

58 originally suggested by Zipser (1977) that the downdrafts in the convective part of a system,

59 referred to in the literature as convective-scale downdrafts, are saturated and the downdrafts in

60 the trailing stratiform region (referred to as mesoscale downdrafts) are unsaturated. Studies with

61 large-eddy simulations (LES; Hohenegger and Bretherton 2011; Torri and Kuang 2016) indicate,

62 however, that most convective downdrafts are unsaturated, consistent with evidence that the

63 evaporation of raindrops within the downdraft likely does not occur at a sufficient rate to

64 maintain saturation (Kamburova and Ludlam 1966).

65   More recently, studies have shown the importance of downdraft parameters in

66 maintaining an accurate simulation of tropical climate in global climate models (GCMs;

67 Maloney   and   Hartmann   2001;   Sahany   and   Nanjundiah   2008;   Del Genio et al.   2012;

2

74 Langenbrunner and Neelin 2017). Accurate simulation of MCSs in continental regions (Pritchard
75 et al. 2011) was also shown to be sensitive to downdraft–boundary layer interactions, with
76 significantly improved representation of MCS propagation in the central US once such
77 interactions were resolved. Additionally, representing the effects of downdrafts and cold pools in
78 models has been shown to have positive effects on the representation of the diurnal cycle of
79 precipitation (Rio et al. 2009; Schlemmer and Hohenegger 2014).

80   This study aims to characterize downdrafts in a comprehensive way in the Amazon for
81 both isolated and mesoscale convective systems, and to provide useful guidance for downdraft
82 parameterization in GCMs. Data from the DOE–Brazil Green Ocean Amazon (GOAmazon)
83 campaign (2014–2015; Martin et al. 2016) provide an unprecedented opportunity to evaluate
84 downdraft characteristics in the Amazon with sufficiently large datasets for quantifying robust
85 statistical relationships describing leading order processes for the first time. Relationships
86 explored previously, primarily in tropical oceanic (Barnes and Garstang 1982; Feng et al. 2015;
87 de Szoke et al. 2017) or mid-latitude regions (Charba 1974; Engerer et al. 2008), such as time
88 composites of wind and thermodynamic quantities relative to downdraft precipitation, are also
89 revisited and compared to our findings over the Amazon. Downdrafts in MCSs and isolated cells
90 are compared to inform decisions concerning their unified or separate treatment in next
91 generation models. The effect of downdrafts on surface thermodynamics and boundary layer
92 recovery are examined, and the origin height of the downdrafts explored, combining inferences
93 from radar wind profiler data for vertical velocity and thermodynamic arguments from simple
94 plume models. Lastly, statistics describing cold pool characteristics at the surface are presented
95 and discussed for possible use as model diagnostics.

96 **2 Data and Methods**

97   Surface meteorological values (humidity, temperature, wind speed, precipitation) were
98 obtained from the Aerosol Observing meteorological station (AOSMET) at the DOE ARM site
99 in Manacapuru, Brazil, established as part of the GoAmazon2014/5 campaign. The record used
100 in this study spans 10 Jan 2014–20 Oct 2015. Values in this study are averaged at 30-min
101 intervals. Equivalent potential temperature is computed following Bolton (1980).

102   Thermodynamic profiles are obtained from radiosonde measurements within 6 h of a
103 convective event. Radiosondes are launched at approximately 01:30, 7:30, 13:30, and 19:30 LT
104 each day, with occasional radiosondes at 10:30 LT in the wet season. Profiles of vertical velocity

Comment [ks1]:

3

105 and radar reflectivity are obtained from a 1290 MHz radar wind profiler (RWP) reconfigured for
106 precipitation modes. It has a beam width of 6° (~ 1 km at 10 km AGL), a vertical resolution of
107 200 m, and a temporal resolution of 6 seconds (Giangrande et al. 2016).

108   Precipitation data at 25 km and 100 km, as well as convection classifications, are derived
109 from an S-Band radar located approximately 67 km to the northeast of the primary
110 GoAmazon2014/5 site (T3) at the Manaus Airport. Composite constant altitude low-level
111 gridded reflectivity maps (constant altitude plan position indicators, CAPPIs) were generated,
112 and the radar data were gridded to a Cartesian coordinate grid with horizontal and vertical
113 resolution of 2 km and 0.5 km, respectively. Rain rates were obtained from the 2.5 km
114 reflectivity using the reflectivity-rain rate (Z-R) relation $Z=174.8R^{1.56}$ derived from disdrometer
115 data. The spatially averaged rainfall rate over a 25 km and 100 km grid box were used in this
116 study. The center of the 100 km grid box is shifted slightly to the right of center with respect to
117 the T3 site due to reduced data quality beyond a 110 km radius.

118   All MCSs and isolated cells composited produce downdrafts that create a subsequent
119 drop in θ_e at the surface of more than 5 K in a 30-min period and have precipitation rates
120 exceeding 10 mm h^{-1} within that same period. These criteria were chosen to examine the most
121 intense downdraft events with the most well-defined vertical velocity signatures in the RWP
122 data. Only data for events with complete vertical velocity data coverage over the 1 h period
123 spanning the passage of the convective cells and centered around the maximum precipitation
124 were composited and evaluated.

125   Isolated convective cells were identified by S-Band composite reflectivity, as in Fig. 1,
126 and are defined as being less than 50 km in any horizontal dimension (contiguous pixels with
127 reflectivity > 30 dBZ) with a maximum composite reflectivity of greater than or equal to 45 dBZ.
128 Following the criteria defined above, this resulted in the selection of 11 events, all of which were
129 in the late morning or afternoon hours between 11:00 and 18:00 LT. Mesoscale convective
130 systems follow the traditional definition of regions of contiguous precipitation at scales of 100
131 km or greater (contiguous pixels with reflectivity > 30 dBZ) in any horizontal dimension (e.g.
132 Houze 1993; Houze 2004). All of the events sampled are characterized by a leading edge of
133 convective cells with a trailing stratiform region (Fig. 1), which is the most common MCS type
134 (Houze et al. 1990). The above criteria yielded 18 events: 11 in the late morning and early

4

Deleted: convective events used in this study meet the following criteria:

Deleted: producing

Deleted: less

Deleted: $^{\circ}$ C

Deleted: having

141 afternoon hours (11:00-18:00 LT) and 6 in the late evening/early morning hours (22:00-11:00

142 LT).

143   In Sect. 6, statistics are presented using nearly the entire two-year timeseries of

144 meteorological variables at the GoAmazon2014/5 site, as well as 15 years of data (1996–2010)

145 from the DOE ARM site at Manus Island in the tropical western Pacific. One-hour averages are

146 computed in $\Delta\theta_e$ and precipitation.

147 **3 Surface Thermodynamics**

148   Composites of surface meteorological variables are displayed in Fig. 2 for the 11 isolated

149 cellular deep convective events coinciding with drops in equivalent potential temperature of 5 K

150 or greater and precipitation rates greater than 10 mm h^{-1} (see Sect. 2). The composites are

151 centered 3 h before and after the 5-min interval marking the sharpest decrease in surface θ_e in

152 the mean timeseries (time 0). All timeseries averaged in the composites are shifted to the mean

153 value at the θ_e minimum and shading on the composites shows +/- 1 standard deviation for

154 anomalies with respect to the θ_e minimum to provide a sense of the variability. All differences

155 quoted are the differences between the maximum and minimum values within the 1 h timeframe

156 of convective cell passage (+/- 30 min of time 0), unless noted otherwise. Recovery percentages

157 are computed as the difference between the minimum and maximum values between time 0 and

158 some specified time afterwards, divided by the difference between the minimum and maximum

159 values within 30 minutes of time 0.

160   In the two hours leading isolated convection, the CWV increases by 4.5 mm. The mean

161 value of θ_e 30 minutes before the minimum recorded θ_e are 353.7 K. As the systems pass, the θ_e

162 mean value drops by an average 9.6 K to an average value of 344.2 K. Since the isolated

163 convective cells observed occur in the daytime hours, the relative humidity is seen to drop

164 steadily throughout the 3 h period leading the convection following the rise in temperatures with

165 the diurnal cycle. The mean relative humidity (RH) rises to 82.3% within 30 minutes of system

166 passage, which indicates that the downdrafts are sub-saturated when they reach the surface.

167 Within the hour, temperatures drop by 4.2 K to 24.7 K, which is a smaller decrease than observed

168 over mid-latitude sites (see Table 2 in Engerer et al. 2008 for a review of mid-latitude case

169 studies) and specific humidity drops by 1.5 g kg^{-1} to 15.7 g kg^{-1}. Mean winds reach 6.4 m s^{-1},

170 consistent with previous studies that document strong horizontal winds associated with the

5

Deleted: C

Deleted: less

Deleted: 0.5 h

Deleted: 3

Deleted: 353.6° C

Deleted: 8.9° C

Deleted: 7° C

Deleted: 1

Deleted: 6

Deleted: 4° C

Deleted: 9° C

Deleted: 1

Deleted: 6.0

Deleted: 5.5

185 leading edges of cold pools (e.g. Fujita 1963; Wakimoto 1982), but are lower than the observed

186 values for mid-latitude storms (Engerer et al. 2008). Additionally, surface pressure often

187 increases with the existence of a cold pool and is referred to as the meso-high (Wakimoto 1982).

188 Here, it increases marginally by 0.6 hPa, but this value is much less than the typical values

189 observed in mid-latitudes (e.g. Goff 1976; Engerer et al. 2008). Lastly, 32.7% (52.4%) of the

190 temperature and 88.8% (88.9%) moisture depleted by the downdraft recovers within one (two)

191 hour(s) of cell passage, with moisture recovering more quickly and by a greater percentage than

192 temperature. It is likely that moisture recovers more quickly than temperature because of

193 increased evaporation, while cloud cover persistence may continue to affect temperature. It is

194 difficult to observe heat fluxes using eddy covariance techniques during precipitation, however,

195 so we are unable to properly quantify this. Nevertheless, we include measurements of heat fluxes

196 in Supplementary Figs. S1 and S2 to assess general trends.

197 Composites of surface meteorological variables are also shown in Fig. 2 for the 17 MCSs

198 with surface θ_e depressions of 5 K or greater and coincident precipitation rates of 10 mm h^{-1} or

199 greater. On average, the environment is more humid for MCSs than for the isolated cases, as is

200 seen in the CWV composite. CWV between hours -3 and -1 leading the MCSs is higher on

201 average than that observed leading the isolated cells, but increases to a comparable magnitude of

202 ~59 mm within the hour. CWV increases by an average of 1.5 mm in the 2 h leading the passage

203 of MCSs, which is slightly lesser than the increases reported in Taylor et al. 2017 (~4 mm) in the

204 Sahel, though the Amazon is a more humid environment. Values of θ_e leading the passage of

205 MCSs (350.3 K) are 3.4 K lower than the θ_e values leading the isolated cells (353.7 K), mostly

206 due to lower surface temperatures (27.0 K for MCSs vs. 28.9 K for isolated cells). The

207 precipitation occurs over a longer period than in the cases of isolated cells, as there is often

208 stratiform rain trailing the leading convective cells.   The stratiform rain and associated

209 downdrafts also sustain the cooling and drying of the near surface layers for many hours lagging

210 the precipitation maximum. The relative humidity maximum in the cold pool is 90.2% ($\Delta RH =$

211 13.3%), the specific humidity minimum is 15.4 g kg^{-1} ($\Delta q = 1.6$ g kg^{-1}), and the temperature

212 minimum is 22.8° C ($\Delta T = 4.2$ K), with winds gusting to an average of 7.8 m s^{-1} with the passage

213 of the leading convective cells. The cold pools are thus cooler, drier, and nearer to saturation for

214 the MCSs than for the isolated cells. It is worth noting that these statistics for MCSs are not

215 greatly affected by the inclusion of nighttime events; composites for afternoon only MCSs yield

6

228 similar results. Overall, on average, the environments in which MCSs live are moister, they have

229 colder, drier cold pools that are nearer to saturation, the winds at their leading edges are gustier,

230 and the boundary layer recovers more slowly than for isolated cells.

231 　　　Here, we composite events based on strict criteria identifying the strongest convective

232 events (see Table S1 for dates/times of events composited in Figs. 2-6). In Supplemental Figs. S1

233 and S2, we instead composite based on either a minimum θ_e decrease or a minimum

234 precipitation rate to test the sensitivity of the results presented here and include additional events.

235 We also examine the sensitivity to averaging by compositing timeseries of meteorological

236 variables averaged at 30-min intervals and plot results for 6 h leading and lagging the

237 convection. The features discussed above associated with the passage of isolated systems and

238 MCSs are generally robust to averaging and the choice of imposed criteria.

239 **4 Downdraft Origin and the Effects of Mixing**

240 　　　Many previous studies of moist convective processes use θ_e as a tracer since it is

241 conserved in the condensation and evaporation of water and for dry and moist adiabatic

242 processes (e.g., Emanuel 1994). Tracing surface θ_e to its corresponding value aloft has been used

243 in many studies of tropical convection to examine potential downdraft origin heights (e.g. Zipser

244 1969; Betts 1973, 1976; Betts and Silva Dias 1979; Betts et al. 2002). This assumes that

245 downdraft air conserves θ_e to a good approximation and that downdraft air originates at one

246 height above ground level. Neither of these assumptions is likely to be true, as mixing is likely

247 occurring between the descending air and the environmental air and thus originating from

248 various levels. However, it can provide a useful reference point for further considerations.

249 　　　We examine the mean θ_e profiles to place bounds on mixing and downdraft origin with

250 simple thermodynamic arguments and plume computations. The profiles composited in Fig. 3

251 were measured within the 6 hours prior to the same MCSs and isolated events composited in Fig.

252 2, less two MCS events that did not have corresponding radiosonde measurements. Simply

253 matching the mean of the minimum θ_e value within the cold pools to the minimum altitude at

254 which those values are observed yields 2.1 km for MCSs (left panel, Fig. 3) and 1.5 km for

255 isolated cells (right panel, Fig. 3). Again, this assumes that θ_e is conserved and that the air

256 originates at one altitude. If instead we assume that substantial mixing occurs with the

257 surrounding environment and that air originates at multiple levels in the lower troposphere, it

Deleted: equivalent

Comment [ks3]:

259 would be plausible for more of the air reaching the surface to originate at altitudes greater than
260 1.5 and 2.1 km for isolated cells and MCSs, respectively. This has been alluded to in previous
261 studies (e.g. Zipser 1969; Gerken et al. 2016), which provide evidence that air originates in the
262 middle troposphere.

263   To examine this, we mix air from above the altitude where the θ_e matched the surface
264 value (shown in the composites in Fig. 2) downward towards the surface, varying the
265 entrainment rate (constant in pressure coordinates). To start, we use a mixing of 0.001 hPa^{-1}, as
266 this is the constant entrainment value used in Brown and Zhang (1997) and Holloway and Neelin
267 (2009), which can produce realistic updraft buoyancy profiles over tropical oceans given
268 simplified assumptions about freezing (no freezing) and condensate loading (all condensate
269 retained). For the MCS case, it is plausible that a downdraft could originate at a height of 2.5 km
270 given this rate of mixing to reach the surface with characteristics given by Fig. 2. If instead the
271 air were coming from the level of minimum θ_e ($\geq$ 3.2 km, on average), an assumption similar to
272 that made by many downdraft parameterizations (e.g. Zhang and McFarlane 1995; Tiedtke 1989;
273 Kain and Fritsch 1990), mixing would need be 2 times greater. For the isolated cells, mixing
274 rates appear to need to be greater in order to produce results consistent with cold pool
275 characteristics at the surface. If we start out at 0.002 hPa^{-1}, the rate sufficient for a minimum θ_e
276 origin for the MCSs, this only yields an origin height of 1.7 km. If instead we assume the air
277 originates somewhere near the level of minimum θ_e, mixing would need to be at least 0.004 hPa^{-}
278 ^{1}. For simplicity the discussion above is in terms of mean profiles – the standard error of the
279 profiles is shown at 50 mb intervals – but computation based on individual profiles yields a
280 standard error in the inferred mixing up about 0.0005 hPa^{-1}. For reference, in the European
281 Center for Medium Range Weather Forecasting Integrated Forecasting System (ECMWF IFS)
282 and Goddard Institute for Space Studies (GISS) Model E2 GCM (Kim et al. 2013), downdrafts
283 mix at a rate of 2 x 10^{-4} m^{-1} (roughly equivalent to 0.002 hPa^{-1} in pressure coordinates in the
284 lower troposphere).

285   To summarize, this analysis is suggestive of bounds on mixing coefficients for downdraft
286 parameterizations. If downdrafts of both convective types mix at similar rates, these results
287 suggest that downdrafts from isolated cells originate at lower levels than MCSs, on average. If
288 instead downdrafts originate from the level of minimum θ_e, mixing rates of 0.002 hPa^{-1} for
289 MCSs and 0.004 hPa^{-1} for isolated convection would be consistent with mean thermodynamic

Comment [ks4]:

290 conditions. In Sections 5 and 6, we provide a complementary probabilistic perspective on levels
291 of origin.

5 Vertical Velocity and Downdraft Probability

293   Figure 4 composites reflectivity (Z), vertical velocity (w), and the probability of
294 observing downdrafts (w < 0 m s^{-1}) for the 11 cases of isolated cellular convection meeting the
295 minimum $\Delta\theta_e$ criteria of -5 K and minimum precipitation criteria of 10 mm h^{-1}. Time 0 is the
296 time right before the sharpest decrease in θ_e and maximum precipitation (slightly offset from the
297 composites in Fig. 2). A 3 h window is composited for reference, but the interval of primary
298 interest is the 1 h window within which the minimum $\Delta\theta_e$ and maximum precipitation are
299 observed. To highlight the interval of interest, the 1 h intervals leading and lagging this period
300 are masked out.
301   The drop in θ_e is coincident with the passage of the isolated cell and its main updraft and
302 precipitation-driven downdraft. Mean reflectivity exceeding 40 dBZ is observed during this
303 period, as are strong updrafts in the middle-upper troposphere. The cell then dissipates and/or
304 moves past the site within an hour. A downdraft is observed directly below and slightly trailing
305 the updraft core. This is the downdraft that is associated with the largest drop in surface θ_e. As is
306 suggested in the literature, these are mainly driven by condensate loading and evaporation of
307 precipitation and are negatively buoyant. The probability of observing negative vertical velocity
308 (threshold < 0 m s^{-1}) within the 30 minutes of minimum $\Delta\theta_e$ and maximum precipitation is
309 highest in the lower troposphere (0-2 km), consistent with precipitation-driven downdrafts
310 observed in other studies (Sun et al. 1993; Cifelli and Rutledge 1994).
311   There is also a high probability of downdrafts in air near the freezing level (masked out in
312 the vertical velocity retrievals, as there is large error associated with retrievals near the freezing
313 level; Giangrande et al. 2016). It appears likely, however, that these downdrafts are
314 discontinuous in height more often than not, as high probabilities are not observed coincidentally
315 in the lowest levels beneath these downdrafts. These mid-upper level downdrafts are documented
316 in previous studies of MCSs, which suggest that they form in response to the pressure field (e.g.
317 Biggerstaff and Houze 1991), can occur quite close to the updraft (Lily 1960; Fritsch 1975), and
318 are positively buoyant (Fovell and Ogura 1988; Jorgenson and LeMone 1989; Sun et al. 1993).
319 These motions produce gravity waves in the stratosphere, as is discussed in Fovell et al. (1992).

9

Comment [ks5]:

Deleted: ° C

Deleted: observed maxima in the absolute value of

Deleted: upper levels

323   Figure 5 shows the same composites for the 18 MCSs observed. They, too, have high
324   reflectivity (mean > 40 dBZ) in the 30 minutes coincident with the minimum θ_e and a defined
325   updraft extending up to the upper troposphere. Downdrafts occurring coincident with the
326   minimum θ_e are observed directly below the updraft signature in the mean vertical velocity
327   panel, and the probabilities are greatest below the freezing level. There are likely also mesoscale
328   downdrafts in the trailing stratiform region of the MCSs, although difficult to discern here, which
329   Miller and Betts (1977) suggest are more dynamically driven than the precipitation-driven
330   downdrafts associated with the leading-edge convection. These likely sustain the low θ_e air in
331   the boundary layer for hours after the initial drop, observed in Fig. 2. Vertical motions in the
332   stratiform region are weaker than in the convective region, and on average, as in Cifelli and
333   Rutledge (1994), rarely exceed 1 m s^{-1}.

334   Figure 6 is a concise summary of the results presented in Figs. 4 and 5, showing the mean
335   vertical velocity within the 30-min of sharpest $\Delta\theta_e$ for MCSs and isolated cells. Means are for w
336   > 0 m s^{-1} only (updrafts) or w < 0 m s^{-1} only (downdrafts) at each height (as in Giangrande et al.
337   2016) and are thus characteristic of magnitudes rather than bulk air motions. Updraft and
338   downdraft strength increases with height, consistent with results from previous studies evaluating
339   a broader range of conditions (May and Rajopadhyaya 1999; Kumar et al. 2015; Giangrande et
340   al. 2016). The corresponding mean probability of observing such motions at each height is
341   shown in the right panel. Probabilities, which can be interpreted loosely as convective area
342   fractions (Kumar et al. 2015; Giangrande et al. 2016), are largest below the freezing level for
343   downdrafts and in the 3-7 km region for updrafts. The probability of downdrafts for both isolated
344   cells and MCSs increases nearly linearly towards the surface below the freezing level. Thus, this
345   behavior in the lowest 3 km summarizes our results from the previous two figures and suggests
346   that the mean properties of downdrafts are such that air accumulates along descent – analogous
347   to mixing. The probability and vertical velocity for both MCSs and isolated cells correspond to
348   mass flux profiles that increase nearly linearly throughout the lower troposphere for updrafts and
349   that decrease nearly linearly throughout the lower troposphere for downdrafts, as seen in
350   Giangrande et al. (2016) over a broader range of convective conditions. To give some sense of
351   the error in these estimates, Wilson score intervals (lower bound/upper bound) for the 18 MCSs
352   cases are roughly 0.16/0.23 for a probability of 0.7, 0.21/0.21 for a probability of 0.5, and
353   0.23/0.16 for a probability of 0.3; for 11 events (as in the isolated cases), the intervals are

10

roughly 0.19/0.28 for a probability of 0.7, 0.25/0.25 for a probability of 0.5, and 0.28/0.19 for a probability of 0.3.

    These results, and those presented in the previous section, suggest a range of downdraft origin levels throughout the lowest few kilometers within both organized and unorganized convective systems. Several observational studies corroborate the evidence presented here that a majority of the air reaching the surface in deep convective downdrafts originates at low-levels (Betts 1976; Barnes and Garstang 1982; Betts et al. 2002; de Szoke et al. 2017). Betts (1976) concluded that the downdraft air descends approximately only the depth of the subcloud layer (~150 mb). Betts et al. (2002) cited a range of 765-864 hPa for the first levels at which the surface θ_e values matched those of the air aloft. Additionally, there are many modeling studies that provide evidence of these low-level origins (Moncrieff and Miller, 1976; Torri and Kuang, 2016). Recently, Torri and Kuang (2016) used a Lagrangian particle dispersion model to show that precipitation-driven downdrafts originate at very low levels, citing an altitude of 1.5 km from the surface, with the mode of the distribution nearer to 1 km. These conclusions are consistent with our results here, suggesting that downdraft parameterizations substantially weight the contribution of air from the lower troposphere (e.g. with substantial mixing and/or modifying the height of downdraft origin).

6 Relating Cold Pool Thermodynamics to Precipitation

    As seen in previous sections, the passage of both organized and unorganized convection can lead to substantial decreases in θ_e resulting mainly from precipitation-driven downdrafts formed from the leading convective cells. In this section, we search for robust statistical relationships between key thermodynamic variables for potential use in improving downdraft parameterizations in GCMs. These statistics differ from those presented in Figs. 2-6, as these statistics are not conditioned on convection type and sample both precipitating and non-precipitating points within the timeseries analyzed. All data available at the surface meteorological station during the GoAmazon2014/5 campaign from 10 Jan 2014–20 Oct 2015 are included in these statistics.

    The first of these statistics conditionally averages precipitation rate by $\Delta\theta_e$ (Fig. 7), variants of which have been discussed in previous studies (Barnes and Garstang 1982; Wang et al. 2016). Our statistics mimic those shown in previous work relating column-integrated moisture

11

384   to deep convection over tropical land (Schiro et al. 2016) and ocean (Neelin et al. 2009;

385   Holloway and Neelin 2009). The direction of causality in the CWV-precipitation statistics,

386   however, is the opposite of what is presented here. CWV is thought to primarily be the cause of

387   intense precipitation and deep convection, while here the $\Delta\theta_e$ observed is a direct result of the

388   precipitation processes and associated downdraft. Nevertheless, examining the distribution of

389    $\Delta\theta_e$ observed at the surface and magnitudes of the rain rates associated with the largest drops in

390    $\Delta\theta_e$ across different regions in the tropics can place bounds on downdraft behavior. We will also

391   conditionally average $\Delta\theta_e$ by precipitation rate, a more physically consistent direction of

392   causality.

393   Figure 7 shows precipitation rates binned by $\Delta\theta_e$ for in-situ and radar-derived

394   precipitation. Bins are 1 K in width (bins with less than 5 observations are eliminated from the

395   analysis) and precipitating events are defined as having rain rates greater than 2 mm h^{-1}. This

396   threshold is chosen based on results from Barnes and Garstang (1982), who suggested it as a

397   minimum precipitation rate for observing coincident decreases in θ_e at the surface. These

398   statistics mainly suggest that a majority of the substantial decreases in θ_e at the surface occur

399   coincidently with heavy precipitation, which is particularly evident from the sharp increase in

400   probability of precipitation (middle panel).

401   S-Band radar data are averaged in 25 km and 100 km grid boxes surrounding the

402   GoAmazon2014/5 site to examine the precipitation-$\Delta\theta_e$ relation with model diagnostics in mind

403   (Fig. 7). The $\Delta\theta_e$ shown is in situ, since we do not have spatial information in the moisture and

404   temperature fields at a high enough temporal frequency to match the radar data. Out to 25 km,

405   the statistics are very similar to those observed using in situ precipitation. Theoretical (Romps

406   and Jevanjee 2015), modeling (Tompkins 2001; Feng et al. 2015), and observational (Feng et al.

407   2015) studies have all examined typical sizes of cold pools, which can be on the order of 25 km

408   in diameter for any one cell. Cold pools can combine, however, to form a larger, coherent

409   mesoscale-sized cold pool (radius of 50 km or greater), as is commonly associated with

410   mesoscale convective systems (Fujita 1959; Johnson and Hamilton 1988). Therefore, it is likely

411   that our use of the in situ $\Delta\theta_e$, assuming cold pool properties are somewhat homogeneous in

412   space, is appropriate for scales up to 25 km. Beyond this scale, it is likely that the $\Delta\theta_e$ would be

413   smoothed by averaging, particularly for the smaller isolated cells, as would precipitation. For the

414   conditional average precipitation (Fig. 7), this effect may be seen at the 100 km averaging scale.

The probabilities are, however, robust to averaging. This suggests that when drops in θ_e occur locally, there tends to be good correspondence to precipitation both locally and in the surrounding 25 and 100 km averaging areas.

Comment [ks10]:

The width of the distribution of precipitating points is of greatest interest here. The distribution of precipitating points peaks just shy of a $\Delta\theta_e$ of 0 K, indicating that most precipitation events have low rain rates and do not occur coincidently with an appreciable drop in θ_e. The frequency of precipitation drops off roughly exponentially towards lower $\Delta\theta_e$. An interesting feature is the lower bound observed in $\Delta\theta_e$ near -15 K. The mean profiles in Fig. 3 show that, on average, this value of -15 K would be consistent with air originating from the level of minimum θ_e and descending undiluted to the surface. The frequency of observing these values suggests that air very rarely reaches the surface from these altitudes (3 km or higher) undiluted. The θ_e probability distribution is consistent with the results of Sect. 5, indicating that the probability of air from a given level of origin reaching the surface increases toward the surface through the lowest 3 km.

Deleted: ° C

Deleted: ° C

Deleted: ° C

Figure 8 shows remarkable similarity in these statistics when comparing across regions to a DOE ARM site at Manus Island in the tropical western Pacific. As $\Delta\theta_e$ decreases, in situ precipitation rates sharply increase. The PDFs, as well as the steepness and locations of the pickups, are remarkably consistent. Again, the sharpness of these curves is a result of the strongest precipitation events coinciding with the strongest decreases in θ_e, shown in the middle panels in Fig. 8, where the probability of observing coincident precipitation is greatest at low $\Delta\theta_e$.

It is then of interest to see if for a given precipitation rate we can expect a particular $\Delta\theta_e$, as this is the proper direction of causality. Figure 9 conditionally averages $\Delta\theta_e$ by precipitation rate (1-h averages). The minimum $\Delta\theta_e$ and maximum precipitation within a 3-h window are averaged to minimize the effects of local precipitation maxima occurring slightly before or after the maximum in $\Delta\theta_e$. Comparing Fig. 8 and Fig. 9 shows that there can be strong precipitation events without large, corresponding decreases in surface θ_e, but that large decreases in surface θ_e are almost always associated with heavy precipitation. Beyond about 10 mm h^{-1} there is a high probability of observing large, negative $\Delta\theta_e$ and an apparent limit in mean θ_e decreases with rain rate. This makes physical sense, as discussed above (see also Barnes and Garstang 1982), since cooling is limited by the maximum difference between the surface θ_e and the θ_e minimum aloft.

Deleted: maximum

Deleted: minimum

451   The average $\Delta\theta_e$ for rain rates exceeding 10 mm h^{-1} is about -5 K for the Amazon and -4

452 K for Manus Island (Fig. 9). This statistic could be of use in constraining downdraft parameters

453 to be consistent with surface cooling and drying observed in nature. The results for 100 km

454 overlaid in Fig. 9 suggest that even though precipitation rates at 100 km are not simply

455 proportional to in situ rain rates, the main feature of the statistic is robust to averaging

456 precipitation out to a typical GCM grid scale. There are still, however, open questions about

457 scale dependence and how much cooling or drying should be observed for varying space and

458 time scales, given that we are using in situ $\Delta\theta_e$ for all of the statistics presented. Overall, if

459 convective precipitation is present in a GCM grid, a corresponding $\Delta\theta_e$ should result within a

460 range consistent to those observed here, subject to scale dependence.

461   To summarize the results from Figs. 7-9 and provide additional diagnostics, we can ask

462 what fraction of precipitation occurs within a given time window of an appreciable drop in θ_e,

463 and how this fraction changes with precipitation intensity. At the GoAmazon2014/5 site, for

464 $\Delta\theta_e \leq$ -2 K, the fraction of precipitation events within the same hour exceeding 1, 5, 10 mm h^{-1},

465 respectively, is 43%, 63%, and 74%. Similar fractions (though smaller) are found at Manus Isl.:

466 37%, 53%, and 63%, respectively. Increasing the required value of $\Delta\theta_e$ yields smaller fractions –

467 e.g., for $\Delta\theta_e \leq$ -4 K, corresponding fractions at the GoAmazon2014/5 site are about 75% of the

468 above values (37%, 53%, and 62%, respectively). Based on arguments presented above about

469 typical cold pool sizes, these result are likely applicable to GCM grid scales of 0.25^o or less, with

470 evidence of consistency out to 1°.

471 **7 Conclusions**

472   Convective events sampled during the GoAmazon2014/5 campaign compare downdraft

473 characteristics between MCSs and isolated cells and examine their respective effects on surface

474 thermodynamics. All events included in the analysis passed directly over the GoAmazon2014/5

475 site with minimum precipitation rates of 10 mm h^{-1} and $\Delta\theta_e$ less than or equal to -5 K. The

476 isolated events sampled occurred in the afternoon hours only and were characterized by average

477 decreases of 1.5 g kg^{-1} in specific humidity, 4.2 K in temperature, and 9.6 K in θ_e, with an

478 increase of 4.2 m s^{-1} in wind speed at the surface. More than half (59%) of the deficit in θ_e

479 observed with the passage of the cells recovers within 1 h, on average, with the moisture

480 recovering faster than temperature and constituting a larger fraction of the total θ_e recovered.

14

Deleted: ^{o}C

Deleted: ^{o}

Deleted: C

Comment [ks11]:

Deleted: ^{o}C

Deleted: 1

Deleted: 3.9

Deleted: ^{o}C

Deleted: 8.0

Deleted: ^{o}C

Deleted: 5.5

Deleted: 2

492 MCSs show similar decreases in temperature (4.2 K), moisture (1.6 g kg^{-1}), and thus θ_e (9.7 K)

493 at the surface. The θ_e recovers more slowly for MCSs due to the mesoscale downdrafts and

494 associated precipitation in their trailing stratiform regions.

495   Vertical velocity profiles from a radar wind profiler show that the probability of

496 observing downdraft air during the 30 minutes of observed minimum $\Delta\theta_e$ increases with

497 decreasing height in the lowest 3 km for both isolated cells and MCSs. This vertical structure of

498 the downdraft probability is consistent with negative vertical velocities originating at various

499 levels within this layer and continuing to the surface. Considering complementary

500 thermodynamic arguments, without mixing, profiles of θ_e suggest that origin levels at average

501 altitudes of 1.4 and 2.1 km for isolated cells and MCSs, respectively, would be consistent with

502 average cold pool θ_e for these cases. A minimum in θ_e is observed between 3 and 7 km, on

503 average, so for air to originate above 3 km, simple plume calculations suggest that downdrafts in

504 MCSs would have to be mixing with environmental air at an approximate rate of 0.002 hPa^{-1}

505 along descent and at a rate roughly 2 times greater (0.004 hPa^{-1}) for isolated cells. This would

506 imply mass entering the downdraft throughout the lowest few kilometers. Overall the vertical

507 velocity and thermodynamic constraints are consistent in suggesting a spectrum of downdraft

508 mass origin levels throughout the lowest few kilometers.

509   Robust statistical relationships between $\Delta\theta_e$ and precipitation are examined from nearly

510 two years of data at the GoAmazon2014/5 site and 15 years of data at the DOE ARM site at

511 Manus Island in the tropical western Pacific. We conditionally average precipitation by $\Delta\theta_e$,

512 similar to the statistics of precipitation conditioned on a thermodynamic quantity we consider for

513 convective onset statistics. Here, however, the most likely direction of causality differs in that

514 the θ_e drop is caused by the downdraft that delivers the precipitation (as opposed to the

515 thermodynamic profile providing convective available potential energy for an updraft). For in

516 situ precipitation, the conditional average precipitation exhibits a sharp increase with decreasing

517 $\Delta\theta_e$, which is similar in magnitude over land and ocean, reaching roughly 10 mm hour^{-1} at a $\Delta\theta_e$

518 of -10 K. For area-averaged precipitation on scales typical of GCM grids, precipitation

519 magnitudes are smaller for strong, negative $\Delta\theta_e$, consistent with events with large $\Delta\theta_e$ occurring

520 at localized downdraft locations within a larger system with smaller area-average precipitation.

521 The probability distributions of $\Delta\theta_e$ (for precipitating and non-precipitating points) over land and

522 ocean are also remarkably similar. Distributions show exponentially decreasing probability with

Deleted: 3
Deleted: 7
Deleted: ° C
Deleted: but larger decreases in
Deleted: 5
Deleted: 1
Deleted: ° C)
Deleted: O
Deleted: ° C
Deleted: the points

decreasing $\Delta\theta_e$, providing additional evidence that downdraft plumes originating in the lowest levels are orders of magnitude more likely than plumes descending with little mixing from the height of minimum θ_e. Conditionally averaging $\Delta\theta_e$ by precipitation (the most likely direction of causality) suggests an average limit in $\Delta\theta_e$ of -4 K to -5 K given high precipitation typical of downdraft conditions. The corresponding 90th percentile yields $\Delta\theta_e$ of roughly -10 K, consistent with results obtained from composting strong downdrafts. The robustness of these statistics over land and ocean, and to averaging in space at scales appropriate to a typical GCM resolution, suggests possible use of these statistics as model diagnostic tools and observational constraints for downdraft parameterizations.

Acknowledgments

| Deleted: ° C |
| Deleted: ° C |
| Deleted: ° C |

16

565   **References**

566   Atmospheric Radiation Measurement (ARM) Climate Research Facility. 2013(a), updated
567   hourly. Meteorological Measurements associated with the Aerosol Observing System
568   (AOSMET). 2014-01-10 to 2015-10-20, ARM Mobile Facility (MAO) Manacapuru,
569   Amazonas, Brazil; MAOS (S1). Compiled by A. Koontz, J. Kyrouac and S. Springston.
570   Atmospheric Radiation Measurement (ARM) Climate Research Facility Data Archive:
571   Oak Ridge, Tennessee, USA. Data set accessed at http://dx.doi.org/10.5439/1025153.

572   Atmospheric Radiation Measurement (ARM) Climate Research Facility. 2013(b), updated
573   hourly. Balloon-Borne Sounding System (SONDEWNPN). 2014-01-10 to 2015-10-
574   20, ARM Mobile Facility (MAO) Manacapuru, Amazonas, Brazil; AMF1 (M1).
575   Compiled by D. Holdridge, J. Kyrouac and R. Coulter. Atmospheric Radiation
576   Measurement (ARM) Climate Research Facility Data Archive: Oak Ridge, Tennessee,
577   USA. Data set accessed at http://dx.doi.org/10.5439/1021460.

578   Atmospheric Radiation Measurement (ARM) Climate Research Facility. 2014, updated hourly.
579   Eddy Correlation Flux Measurement System (30ECOR). 2014-04-03 to 2015-10-20,
580   ARM Mobile Facility (MAO) Manacapuru, Amazonas, Brazil; AMF1 (M1). Compiled
581   by D. Cook. Atmospheric Radiation Measurement (ARM) Climate Research Facility
582   Data   Archive: Oak   Ridge,   Tennessee,   USA.   Data   set   accessed   at
583   http://dx.doi.org/10.5439/1025039.

584   Atmospheric Radiation Measurement (ARM) Climate Research Campaign Data, Observations
585   and Modeling of the Green Ocean Amazon (GOAMAZON), 2015. SIPAM Manaus S-
586   Band Radar. 10 Jan 2014–20 Oct 2015, 36° 3.1489^o S, 59.9914° W, Manaus, Amazonas,
587   Brazil (T1). Processed by C. Schumacher. Data set accessed Feb 2017
588   at iop.archive.arm.gov.

589   Atmospheric Radiation Measurement (ARM) Climate Research Facility Observations and
590   Modeling of the Green Ocean Amazon (GOAMAZON), 2015. Radar Wind Profiler
591   (1290RWPPRECIPMOM). Atmospheric Radiation Measurement (ARM) Climate
592   Research Facility Data Archive: Oak Ridge, Tenn. http://dx.doi.org/**10.5439/1256461**

593   Barnes, G. M. and M. Garstang, 1982: Subcloud Layer Energetics of Precipitating Convection.
594   *Monthly Weather Review*, **110**, 102-117.

17

595   Betts, A., 1973: Non-precipitating cumulus convection and its parameterization. *Quarterly*
596   *Journal of the Royal Meteorological Society*, **99**, 178-196.

597   Betts, A. K., 1976: The thermodynamic transformation of the tropical subcloud layer by
598   precipitation and downdrafts. *Journal of the Atmospheric Sciences*, **33**, 1008-1020.

599   Betts, A. K., and M. F. Silva Dias, 1979: Unsaturated downdraft thermodynamics in
600   cumulonimbus. *Journal of the Atmospheric Sciences*, **36**(6), 1061-1071.

601   Betts, A. K., and C. Jakob, 2002: Study of diurnal cycle of convective precipitation over
602   Amazonia using a single column model, *Journal of Geophysical Research.,* **107**, 4732.

603   Biggerstaff, M. I., and R. A. Houze Jr, 1991: Kinematic and precipitation structure of the 10–11
604   June 1985 squall line. *Monthly Weather Review*, **119**, 3034-3065.

605   Boing, S. J., H J. J. Jonker, A. P. Siebesma, and W. W. Grabowski, 2012: Influence of the
606   Subcloud Layer on the Development of a Deep Convective Ensemble. *Journal of the*
607   *Atmospheric Sciences,* **69**, 2682-2698.

608   Bolton, D., 1980: The computation of equivalent potential temperature. *Monthly Weather*
609   *Review*, **108**, 1046-1053.

610   Byers, H. R. and R. R. Braham, 1949: The thunderstorm: report of the Thunderstorm Project. *US*
611   *Government Printing Office.*

612   Cifelli, R., and S. A. Rutledge, 1994: Vertical motion structure in maritime continent mesoscale
613   convective systems: Results from a 50-MHz profiler. *Journal of the Atmospheric*
614   *Sciences*, **51**, 2631-2652.

615   Del Genio, A. D., Y. Chen, D. Kim, M.-S. Yao, 2012: The MJO Transition from Shallow to
616   Deep Convection in CloudSat/CALIPSO Data and GISS GCM Simulations. *Journal of*
617   *Climate,* **25**, 3755-3770.

618   Emanuel, K. A., 1994: Atmospheric Convection. 1st ed. Oxford University Press, 580 pp.

619   Engerer, N. A., D. J. Stensrud, and M. C. Coniglio, 2008: Surface characteristics of observed
620   cold pools. *Monthly Weather Review*, **136**, 4839-4849.

621   Feng, Z., S. Hagos, A. K. Rowe, C. D. Burleyson, M. N. Martini, and S. P. Szoeke, 2015:
622   Mechanisms of convective cloud organization by cold pools over tropical warm ocean
623   during the AMIE/DYNAMO field campaign. *Journal of Advances in Modeling Earth*
624   *Systems*, **7**, 357-381.

625 Fritsch, 1975: Cumulus dynamics: Local compensating subsidence and its implications for
626   cumulus parameterization. *Pure and Applied Geophysics,* **113***,* 851-867.

627 Fovell, R. G. and Ogura, Y., 1988: Numerical simulation of a midlatitude squall line in two
628   dimensions. *Journal of the Atmospheric Sciences*, **45**, 3846-3879.

629 Fovell, R., D. Durran, and J. R. Holton, 1992: Numerical simulations of convectively generated
630   stratospheric gravity waves. *Journal of the Atmospheric Sciences*, **49**, 1427-1442.

631 Fovell, R. G. and P. H. Tan, 1998: The temporal behavior of numerically simulated multicell-
632   type storms. Part II: The convective cell life cycle and cell regeneration. *Monthly*
633   *Weather Review*, **126**, 551-577.

634 Fujita, T., 1959: Precipitation and cold air production in mesoscale thunderstorm
635   systems. *Journal of Meteorology*, **16**, 454-466.

636 Gerken, T., D. Wei, R. J. Chase, J. D. Fuentes, C. Schumacher, L. Machado, R. V. Andreoli et
637   al., 2016: Downward transport of ozone rich air and implications for atmospheric
638   chemistry in the Amazon rainforest. *Atmospheric Environment,* **124**, 64-76.

639 Giangrande, S. E., T. Toto, M. P. Jensen, M. J. Bartholomew, Z. Feng, A. Protat, C. R. Williams,
640   C. Schumacher, and L. Machado, 2016: Convective cloud vertical velocity and mass-flux
641   characteristics from radar wind profiler observations during GoAmazon2014/5. *Journal*
642   *of Geophysical Research: Atmospheres*, **121**(21).

643 Goff, R., 1976: Vertical structure of thunderstorm outflows. *Monthly Weather Review*, **104**,
644   1429-1440.

645 Hohenegger, C. and C. S. Bretherton, 2011: Simulating deep convection with a shallow
646   convection scheme. *Atmospheric Chemistry and Physics*, **11**(20), 10389-10406.

647 Holloway, C. E., and J. D. Neelin, 2009: Moisture Vertical Structure, Column Water Vapor, and
648   Tropical Deep Convection. *Journal of the Atmospheric Sciences,* **66**, 1665–1683.

649 Houze, R. A., B. F. Smull, and P. Dodge, 1990: Mesoscale organization of springtime rainstorms
650   in Oklahoma. *Monthly Weather Review*, **118**, 613-654.

651 Houze, R.A., 1993: *Cloud Dynamics*, 573 pp., Academic, San Diego, Calif.

652 Houze, R. A., 2004: Mesoscale convective systems. *Reviews of Geophysics*, **42**(4).

653 Johnson, R. H., and P. J. Hamilton, 1988: The relationship of surface pressure features to the
654   precipitation and airflow structure of an intense midlatitude squall line. *Monthly Weather*
655   *Review*, **116**, 1444-1473.

19

656 Jorgensen, D. P. and M. A. LeMone, 1989: Vertical velocity characteristics of oceanic
657   convection. *Journal of the Atmospheric Sciences*, **46**, 621-640.

658 Kamburova, P. L. and F. H. Ludlam, 1966: Rainfall evaporation in thunderstorm
659   downdraughts. *Quarterly Journal of the Royal Meteorological Society*, **92**, 510-518.

660 Kain, J. S., and J. M. Fritsch, 1990: A one-dimensional entraining/detraining plume model and
661   its application in convective parameterization. *Journal of the Atmospheric Sciences*, **47**,
662   2784-2802.

663 Khairoutdinov, M., and D. Randall, 2006: High-resolution simulation of shallow-to-deep
664   convection transition over land, *Journal of the Atmospheric Sciences,* **63**, 3421 – 3436.

665 Khairoutdinov, M. F., S. K. Krueger, C. H. Moeng, P. A. Bogenschutz and D. A. Randall, 2009:
666   Large-eddy simulation of maritime deep tropical convection. *Journal of Advances in*
667   *Modeling Earth Systems*, **1**(4).

668 Knupp, K. R. and W. R. Cotton, 1985: Convective cloud downdraft structure: An interpretive
669   survey. *Reviews of Geophysics*, **23**, 183-215.

670 Kumar, V. V., C. Jakob, A. Protat, C. R. Williams, and P. T. May, 2015: Mass-flux
671   characteristics of tropical cumulus clouds from wind profiler observations at Darwin,
672   Australia. *Journal of the Atmospheric Sciences*, **72**, 1837–1855.

673 Langenbrunner, B. and J. D. Neelin: Multiobjective constraints for climate model parameter
674   choices: Pragmatic Pareto fronts in CESM1. *Journal of Advances in Modeling Earth*
675   *Systems*, accepted.

676 Li, Z., P. Zuidema, and P. Zhu, 2014: Simulated convective invigoration processes at trade wind
677   cumulus cold pool boundaries. *Journal of the Atmospheric Sciences*, **71**, 2823-2841.

678 Lily, D., 1960: On the theory of disturbances in a conditionally unstable atmosphere. *Monthly*
679   *Weather Review,* **88**, 1-17.

680 Lima, M. A., and J. W. Wilson, 2008: Convective storm initiation in a moist tropical
681   environment. *Monthly Weather Review*, **136**, 1847-1864.

682 Martin, S. T., P. Artaxo, L. A. T. Machado, A. O. Manzi, R. A. F. Souza, C. Schumacher, J.
683   Wang, M. O. Andreae, H. M. J. Barbosa, J. Fan, G. Fisch, A. H. Goldstein, A. Guenther,
684   J. L. Jimenez, U. Pöschl, M. A. Silva Dias, J. N. Smith, and M. Wendisch, 2016:
685   Introduction: Observations and Modeling of the Green Ocean Amazon
686   (GoAmazon2014/5). *Atmospheric Chemistry and Physics,* **16**, 4785-4797.

20

687   Maloney, E. D. and D. L. Hartmann, 2001: The sensitivity of intraseasonal variability in the
688   NCAR CCM3 to changes in convective parameterization. *Journal of Climate*, **14**, 2015-
689   2034.

690   May, P. T. and D. K. Rajopadhyaya, 1998: Vertical Velocity Characteristics of Deep Convection
691   over Darwin, Australia. *Monthly Weather Review*, **127**, 1056-1071.

692   Miller, M. J., and A. K. Betts, 1977: Traveling convective storms over Venezuela. *Monthly*
693   *Weather Review,* **105**, 833-848.

694   Moncrieff, M. W. and M. J. Miller, 1976: The dynamics and simulation of tropical
695   cumulonimbus and squall lines. *Quarterly Journal of the Royal Meteorological*
696   *Society*, **102**, 373-394.

697   Neelin, J.D., O. Peters, and K. Hales, 2009: The Transition to Strong Convection. *Journal of the*
698   *Atmospheric Sciences,* **66**, 2367–2384.

699   Pritchard, M. S., M. W. Moncrieff, and R. C. Somerville, 2011: Orogenic propagating
700   precipitation systems over the United States in a global climate model with embedded
701   explicit convection. *Journal of the Atmospheric Sciences*, **68**, 1821-1840.

702   Purdom, J. F., 1976: Some uses of high-resolution GOES imagery in the mesoscale forecasting
703   of convection and its behavior. *Monthly Weather Review*, **104**, 1474-1483.

704   Rotunno, R., J. B. Klemp, and M. L. Weisman, 1988: A Theory for Strong, Long-Lived Squall
705   Lines. *Journal of the Atmospheric Sciences,* **45**, 463–485.

706   Rio, C., F. Hourdin, J. Y. Grandpeix, and J. P. Lafore, 2009: Shifting the diurnal cycle of
707   parameterized deep convection over land. *Geophysical Research Letters*, **36**.

708   Romps, D. M., and N. Jeevanjee, 2016: On the sizes and lifetimes of cold pools. *Quarterly*
709   *Journal of the Royal Meteorological Society*, **142**, 1517-1527.

710   Rowe, A. K., and R. A. Houze, Jr., 2015: Cloud organization and growth during the transition
711   from suppressed to active MJO conditions. *Journal of Geophysical Research:*
712   *Atmospheres.*, **120**, 10324–10350.

713   Sahany, S. and R. S. Nanjundiah, 2008: Impact of convective downdrafts on model simulations:
714   results from aqua-planet integrations. In *Annales geophysicae: atmospheres,*
715   *hydrospheres and space sciences* (Vol. 26, No. 7, p. 1877).

21

716 Sahany, S., J. D. Neelin, K. Hales, and R. B. Neale, 2012: Temperature-moisture dependence of
717   the deep convective transition as a constraint on entrainment in climate models. *Journal*
718   *of the Atmospheric Sciences,* **69**, 1340–1358.

719 Schiro, K. A., J. D. Neelin, D. K. Adams, and B. R. Lintner, 2016: Deep Convection and Column
720   Water Vapor over Tropical Land versus Tropical Ocean: A Comparison between the
721   Amazon and the Tropical Western Pacific. *Journal of the Atmospheric Sciences*, **73**,
722   4043-4063.

723 Schlemmer, L., and C. Hohenegger, 2014: The Formation of Wider and Deeper Clouds as a
724   Result of Cold-Pool Dynamics. *Journal of the Atmospheric Sciences,* **71**, 2842–2858.

725 Srivastava, R. C., 1987: A model of intense downdrafts driven by the melting and evaporation of
726   precipitation. *Journal of the Atmospheric Sciences*, **44**, 1752-1774.

727 Sun, J., S. Braun, M. I. Biggerstaff, R. G. Fovell, and R. A. Houze Jr, 1993: Warm upper-level
728   downdrafts associated with a squall line. *Monthly Weather Review*, **121**(10), 2919-2927.

729 Terai, C. R. and R. Wood, 2013: Aircraft observations of cold pools under marine
730   stratocumulus. *Atmospheric Chemistry and Physics*, **13**(19), 9899-9914.

731 Tiedtke, M., 1989: A comprehensive mass flux scheme for cumulus parameterization in large-
732   scale models. *Monthly Weather Review*, **117**(8), 1779-1800.

733 Tompkins, A. M., 2001: Organization of tropical convection in low vertical wind shears: The
734   role of cold pools. *Journal of the Atmospheric Sciences,* **58**, 1650–1672

735 Torri, G. and Z. Kuang, 2016: A Lagrangian study of precipitation-driven downdrafts. *Journal of*
736   *the Atmospheric Sciences*, **73**(2), 839-854.

737 Wakimoto, R. M., 1982: The life cycle of thunderstorm gust fronts as viewed with Doppler radar
738   and rawinsonde data. *Monthly Weather Review*, **110**(8), 1060-1082.

739 Wang, H. and G. Feingold, 2009: Modeling mesoscale cellular structures and drizzle in marine
740   stratocumulus. Part I: Impact of drizzle on the formation and evolution of open
741   cells. *Journal of the Atmospheric Sciences*, **66**, 3237-3256.

742 Wang, J., R. Krejci, S. Giangrande, C. Kuang, H.M. Barbosa, J. Brito, S. Carbone, X. Chi, J.
743   Comstock, F. Ditas, and J. Lavric, 2016: Amazon boundary layer aerosol concentration
744   sustained by vertical transport during rainfall. *Nature,* **539**, 416-419.

22

745 Weisman, M. L., and J. B. Klemp, 1986: Characteristics of isolated convective storms.
746   In *Mesoscale Meteorology and Forecasting* (pp. 331-358). American Meteorological
747   Society.
748 Wilson, J. W., and W. E. Schreiber, 1986: Initiation of convective storms at radar-observed
749   boundary-layer convergence lines. *Monthly Weather Review*, **114**(12), 2516-2536.
750 Zhang, G. J., and N. A. McFarlane, 1995: Sensitivity of climate simulations to the
751   parameterization of cumulus convection in the Canadian Climate Centre general
752   circulation model. *Atmosphere-ocean,* **33**, 407-446.
753 Zipser, E. J., 1969: The role of organized unsaturated convective downdrafts in the structure and
754   rapid decay of an equatorial disturbance. *Journal of Applied Meteorology*, **8**, 799-814.
755 Zipser, E. J., 1977: Mesoscale and convective–scale downdrafts as distinct components of squall-
756   line structure. *Monthly Weather Review*, **105**, 1568-1589.
757 Zuidema, P., Z. Li, R. J. Hill, L. Bariteau, B. Rilling, C. Fairall, W. A. Brewer, B. Albrecht, and
758   J. Hare, 2012: On trade wind cumulus cold pools. *Journal of the Atmospheric
759   Sciences*, **69**, 258-280.

760

761

762

763

764

765

766

767

768

769

770   **Figures**
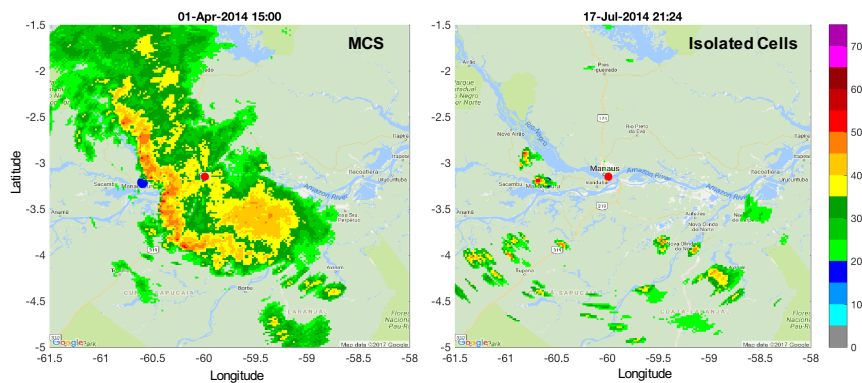
771

772   **Figure 1: Reflectivity (dBZ) from S-Band Radar on 01 Apr 2014 at 15:00 UTC (11:00 LT)**

773   **before the passage of an MCS, and at 17 Jul 2017 at 21:24 UTC (17:24 LT) after the**

774   **passage of an isolated cell. The red dot indicates the location of the S-Band radar, and the**

775   **blue dot indicates the location of the main GOAmazon site (T3).**
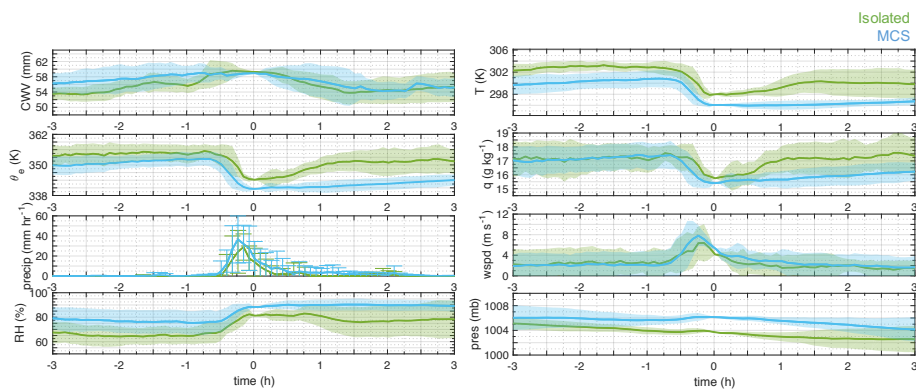
776

777   **Figure 2: Composites of meteorological variables from the AOSMET station at site T3 3 h**

778   **leading and 3 h lagging the minimum in equivalent potential temperature (0 h; 2nd panel)**

779   **coincident with the passage of isolated cells (green) and MCSs (blue). Shading denotes +/- 1**

780   **standard deviation of anomalies with respect to 0 h; bars on precipitation are +/- 1**

24

standard deviation for each time interval. Standard errors would be smaller by a factor of
0.3 for isolated cells and 0.2 for MCSs.
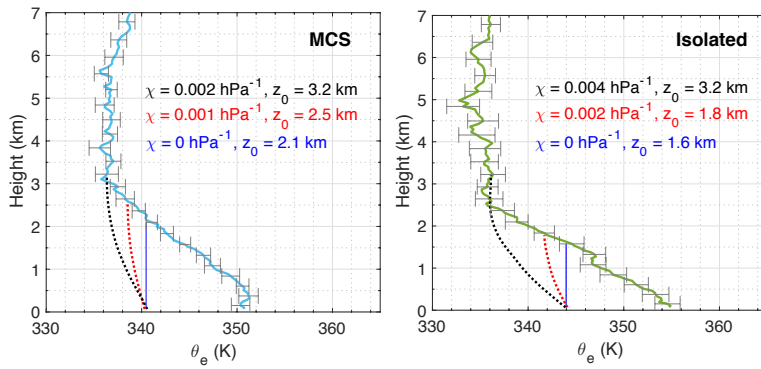
Figure 3: Mean profiles of θ_e within 6 h leading the passage of a deep convective event for MCSs (16 profiles; left) and isolated cells (11 profiles; right). Dashed lines indicate the mean descent path for plumes originating at various altitudes and mixing with the environment at various rates; solid blue line shows mean descent without mixing. Error bars are +/- 1 standard error.

25

791
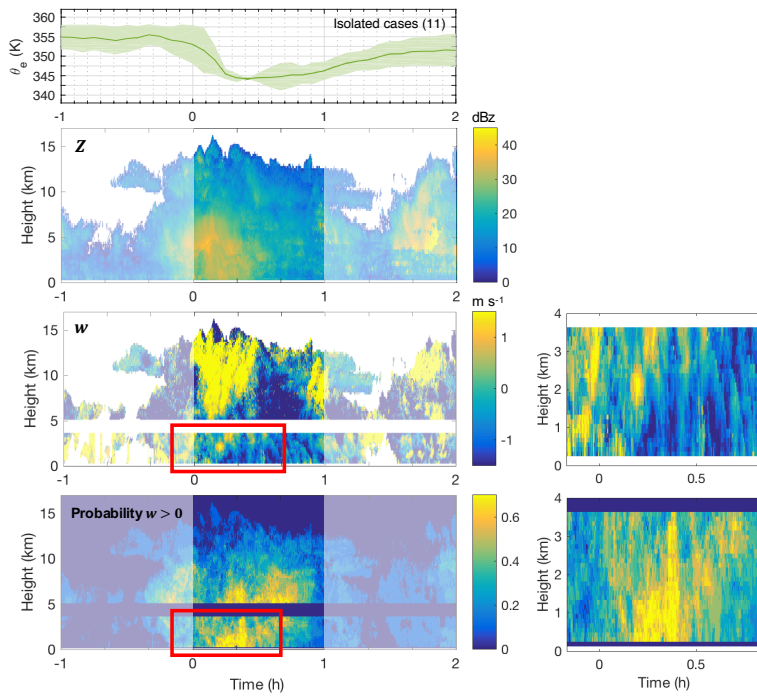
Figure 4: The composite θ_e (K; top panel), mean reflectivity (dBZ; second panel), mean vertical velocity (third panel; m s^{-1}), and probability of w < 0 m s^{-1} (bottom panel) observed by the radar wind profiler at T3 leading and lagging the passage of isolated cells. Plots of w and probability zoomed in time and height (as outlined in red) are shown to the right of the corresponding plots for visual clarity.

26
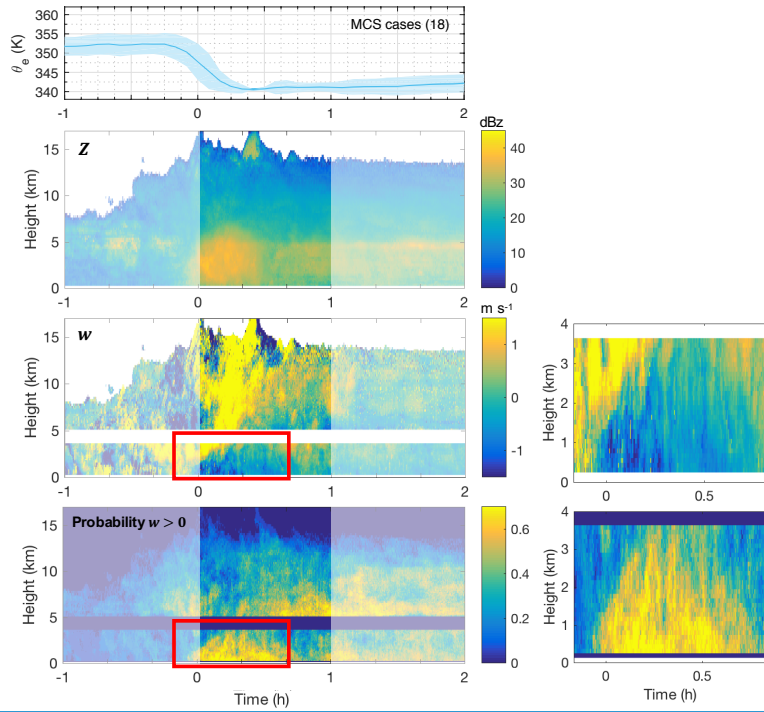
797

798   **Figure 5: Same as Fig. 5, but leading and lagging the passage of MCSs.**

799

800

27
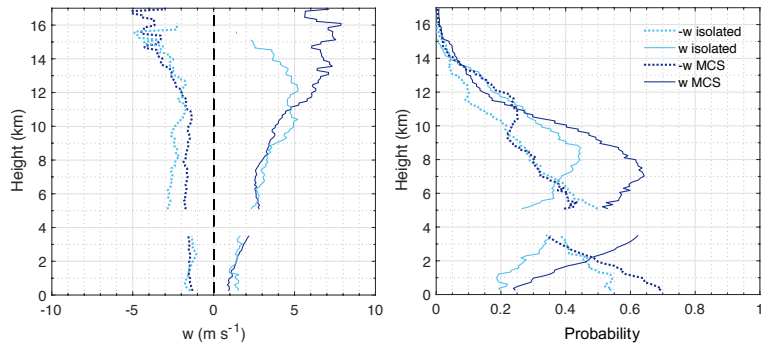
801 **Figure 6: (left) Mean vertical velocity profiles for MCSs and isolated cells for downdrafts**
802 **(w < 0 m s^{-1}; dashed) and updrafts (w > 0 m s^{-1}; solid). (right) Mean probability of**
803 **observing updrafts or downdrafts as a function of altitude. Means are composited from**
804 **data in the 30 minutes of largest drop in $\Delta\theta_e$ (0-0.5 h in Figs. 4 and 5).**
805
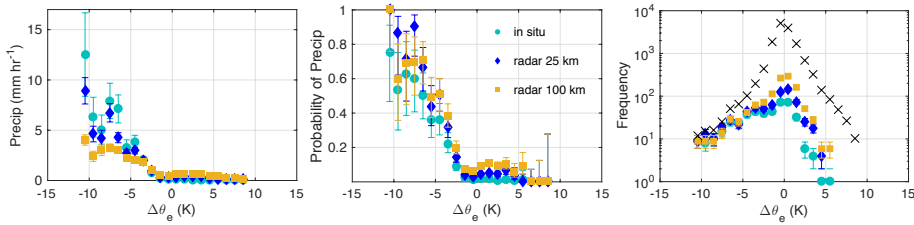
806
807 **Figure 7: (left) Precipitation (1-h averages) conditionally averaged by coincident changes in**
808 **equivalent potential temperature ($\Delta\theta_e$) at the GOAmazon site. Precipitation values**
809 **corresponds to the θ_e values at the end of each differencing interval. Bins are a width of 1°**
810 **and error bars represent the standard error. (middle) The probability of precipitation (> 2**
811 **mm h^{-1}) occurring for a given $\Delta\theta_e$. Error bars represent Wilson score intervals from 5-**
812 **95%. (right) The frequency of occurrence of $\Delta\theta_e$ and precipitation for a given $\Delta\theta_e$**
813 **(precipitation > 2 mm h^{-1}). Precipitation derived from S-Band radar reflectivity at spatial**
814 **averages over 25 km and 100 km grid boxes surrounding the GOAmazon site are included**
815 **for comparison to the in situ precipitation.**
816
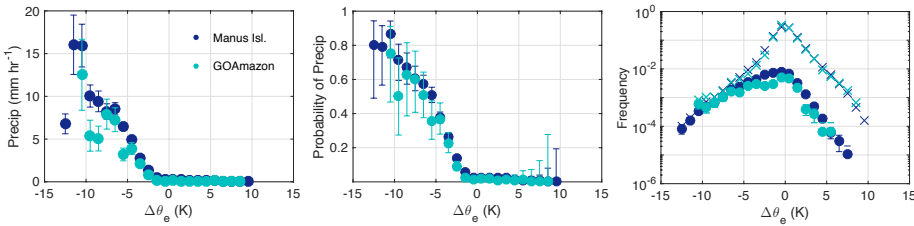
817
818 **Figure 8: Same as Fig. 7, except comparing results from in situ data only at the**
819 **GoAmazon2014/5 site (aqua) and the DOE ARM site at Manus Island (navy).**
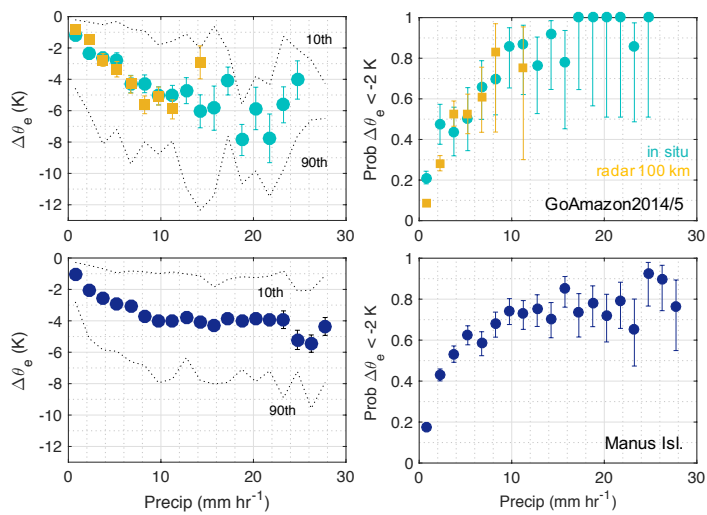
Figure 9: $\Delta\theta_e$ conditionally averaged by coincident precipitation (1-h averages) at the GOAmazon site (top) and at Manus Island (bottom). Precipitation values corresponds to the θ_e values at the end of each differencing interval. Bins are a width of 1.5 mm hr^{-1}. Error bars represent the standard error (left panels), and the 10th and 90th percentile values for each bin are drawn for reference (right panels). Error bars on the probability represent Wilson score intervals from 5-95%.

29